Supplementary Material

Insight into the dynamic transformation properties of microplastic-derived dissolved organic matter and its contribution to the formation of chlorination disinfection by-products

Yingyue Zhou*, Feng Zeng, Kunyan Cui, Longxia Lan, Hao Wang, Weiqian Liang*

*Corresponding authors

School of Chemistry, Sun Yat-sen University, Guangzhou 510000, China

E-mail: qian378378@163.com

Zhou-Yingyue@hotmail.com

Phone: 020-84114133

Characterization methods

The UV absorbance of the PSMPs-DOM was measured in 1 cm quartz cuvettes between 200 and 800 nm at a wavelength step size of 1nm with ultrapure water as blank. The absorption coefficient α(λ) (m^{-1}) was calculated using the equation (Helms et al., 2008) :

$$\alpha(\lambda)=2.303A_{\lambda}/L$$

where A_{λ} is the absorbance at the position λ(nm), and L is the optical path diameter (0.01m).

The spectral slope (S, nm^{-1}) was obtained by a non-linear exponential decay model, and $S_{275-295}$ was the S value at wavelengths of 275-295 nm (Helms et al., 2008). This value was used to characterize the relative molecular size of the DOM.

$$\alpha_{\lambda} = \alpha_{\lambda 0}\, e^{-S(\lambda-\lambda 0)}$$

where $\alpha_{\lambda 0}$ is the absorption coefficient at the reference wavelength λ0, and S is the spectral slope.

The PSMPs-DOM solution was freeze-dried using a freeze dryer (Alpha 1-4 LD Plus) before the scanning of the Fourier transform infrared spectrometer. The scan range of FTIR spectroscopy was 400-4000 cm^{-1}, and the scan resolution was 4 cm^{-1}. Each FTIR spectrum was processed with PerkinElmer Spectrum software for baseline correction.

Three-dimensional excitation emission matrix fluorescence spectra (3D-EEMs) were taken with the excitation wavelengths ranging from 220 nm to 550 nm (scan interval of 1nm), and the emission wavelengths ranging from 250 nm to 650 nm (scan interval of 5nm) for PSMPs-DOM. In addition, the fluorescence spectrum of the

ultrapure water was measured and subtracted from the EEM spectrum of the DOM to eliminate the Raman scattering effect (Christensen et al., 2005). The synchronous fluorescence spectra were obtained in the wavelength range of 340-650 nm with a constant offset ($\Delta\lambda$ = 120 nm), and the scan interval was 1 nm and the scan speed was 600 nm/min^{-1}.

PARAFAC analysis was performed in MATLAB2021a (MathWorks, USA) using the DOMFluor toolbox (Stedmon and Bro, 2008). Rayleigh and Raman scatters were removed before PARAFAC analysis (Zepp et al., 2004). Split-half analysis, residual analysis, and core consistency analysis were used to validate the model and the number of fluorescent components (Stedmon and Bro, 2008). The values for each PAPAFAC fluorescent component was represented by the maximum fluorescence intensity (F_{max}) (Stedmon and Markager, 2005).

The 2D-COS method was implemented to analyze the FTIR data, and the concentration of chlorination was used as the perturbation variable. 2D-COS analysis can extend the one-dimensional spectrum into two-dimensional spectra to catch the signal peak variation (Noda et al., 2000). The order of change of the functional groups was judged according to the positive/negative cross peaks of the synchronous and asynchronous spectra. The 2D-COS was calculated using the 2D-shige software created by Kwansei-Gakuin University, Japan (Noda, 2006).

The detailed extraction methods of THMs.

After 24 h of chlorination reaction, DBPs were extracted from the samples through

liquid-liquid extraction method based on USEPA 551.1 with some modifications (Koh et al., 2022). 3 mL methyl tert-butyl ether (MTBE) containing 4 g anhydrous sodium sulfate was added to the samples, and the mixed solutions were shaken until the solids were mostly dissolved. After 20 min of settling, 1 mL solution from the organic phase was drawn out for analysis.

Reference

Christensen, J.H., Hansen, A.B., Mortensen, J., Andersen, O., 2005. Characterization and matching of oil samples using fluorescence spectroscopy and parallel factor analysis. Anal. Chem. 77, 2210–2217. https://doi.org/10.1021/ac048213k

Helms, J.R., Stubbins, A., Ritchie, J.D., Minor, E.C., Kieber, D.J., Mopper, K., 2008. Absorption spectral slopes and slope ratios as indicators of molecular weight, source, and photobleaching of chromophoric dissolved organic matter. Limnol. Oceanogr. 53, 955–969. https://doi.org/10.4319/lo.2008.53.3.0955

Koh, K.Y., Chen, Z., Lin, S., Chandra Mohan, K., Luo, X., Chen, J.P., 2022. Leaching of organic matters and formation of disinfection by-product as a result of presence of microplastics in natural freshwaters. Chemosphere 299, 134300. https://doi.org/10.1016/j.chemosphere.2022.134300

Noda, I., 2006. Progress in two-dimensional (2D) correlation spectroscopy. J. Mol. Struct. 799, 2–15. https://doi.org/10.1016/j.molstruc.2006.03.053

Noda, I., Dowrey, A.E., Marcott, C., Story, G.M., Ozaki, Y., n.d. Generalized Two-Dimensional Correlation Spectroscopy.

Stedmon, C.A., Bro, R., 2008. Characterizing dissolved organic matter fluorescence with parallel factor analysis: a tutorial. Limnol. Oceanogr. Methods 6, 572–579. https://doi.org/10.4319/lom.2008.6.572

Stedmon, C.A., Markager, S., 2005. Tracing the production and degradation of autochthonous fractions of dissolved organic matter by fluorescence analysis. Limnol. Oceanogr. 50, 1415–1426. https://doi.org/10.4319/lo.2005.50.5.1415

Zepp, R.G., Sheldon, W.M., Moran, M.A., 2004. Dissolved organic fluorophores in southeastern US coastal waters: correction method for eliminating Rayleigh and Raman scattering peaks in excitation–emission matrices. Mar. Chem. 89, 15–36. https://doi.org/10.1016/j.marchem.2004.02.006

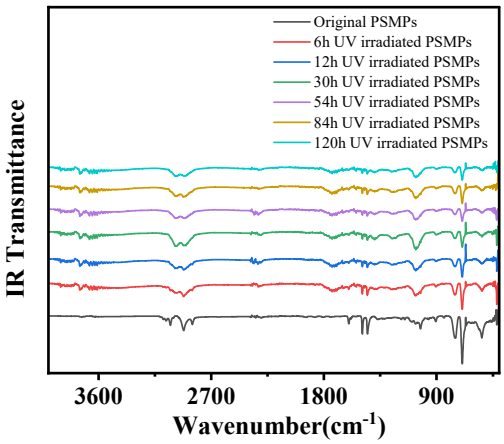

Fig. S1 FTIR spectra of original PSMPs and PSMPs under different UV irradiation time

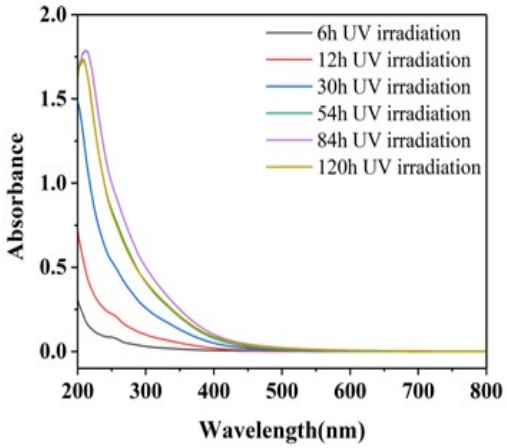

Fig. S2 UV-vis spectra of PSMPs-DOM under and different UV irradiation time

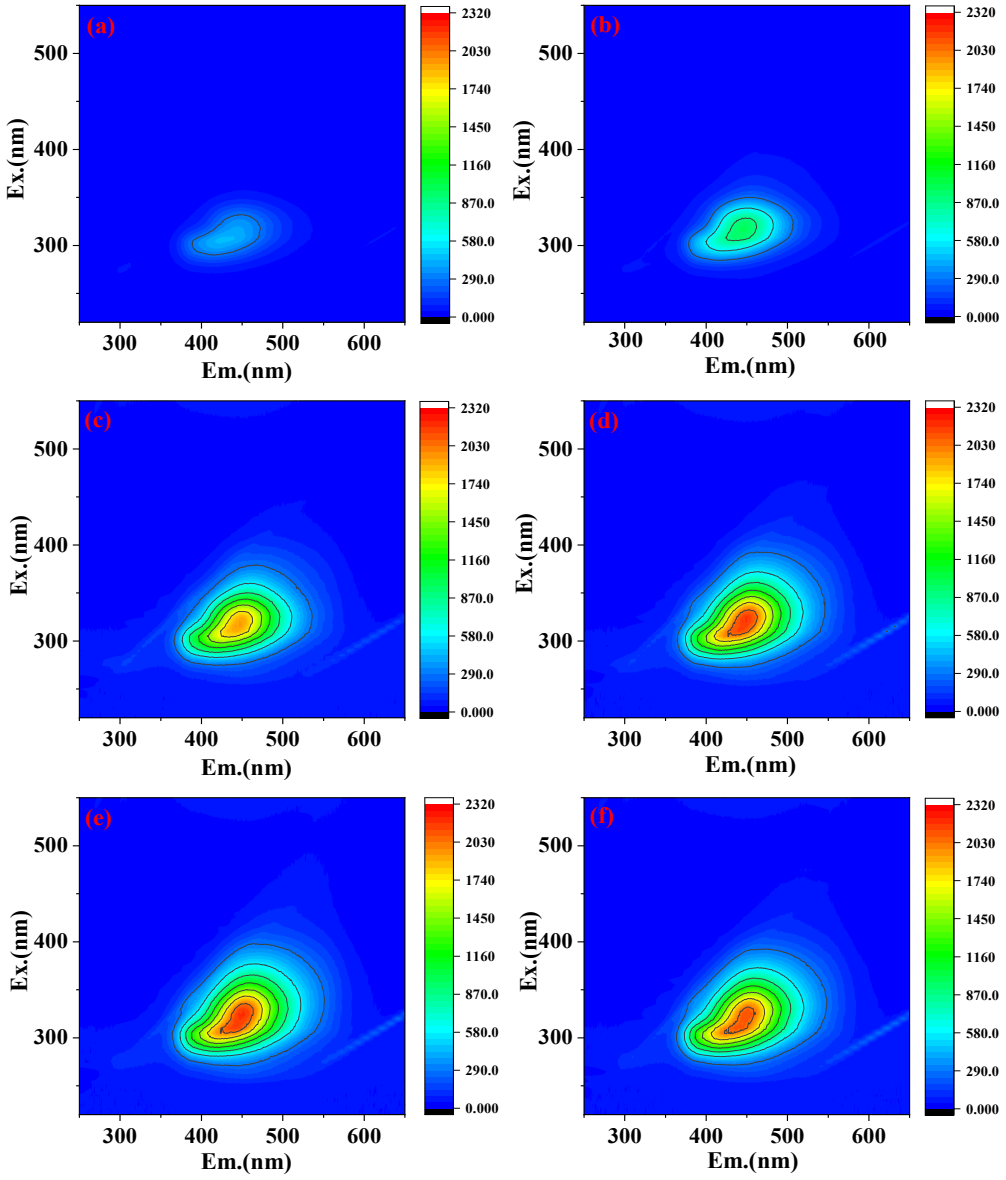

Fig. S3 EEM spectra of PSMPs-DOM under different UV irradiation time ((a)-(f), 6, 12, 30, 54, 84, 120 h)

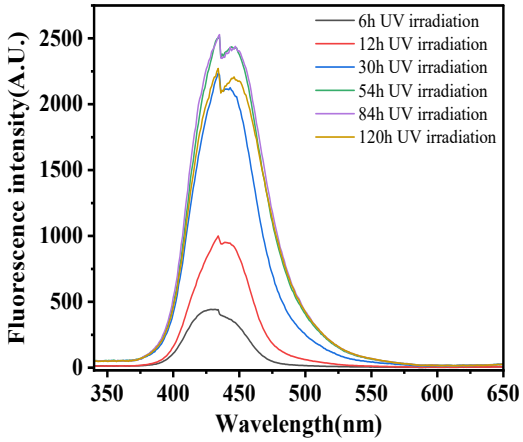

Fig. S4 Synchronous fluorescence spectra of PSMPs-DOM under different UV irradiation time

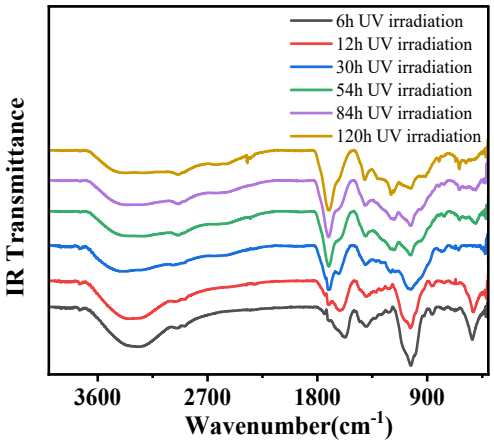

Fig. S5 FTIR spectra of PSMPs-DOM under different UV irradiation time

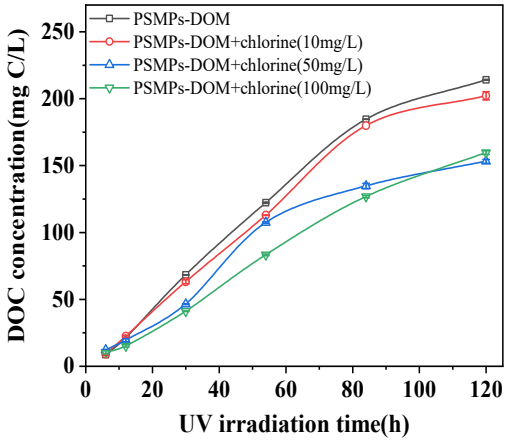

Fig. S6 DOC concentration of PSMPs-DOM before and after chlorination

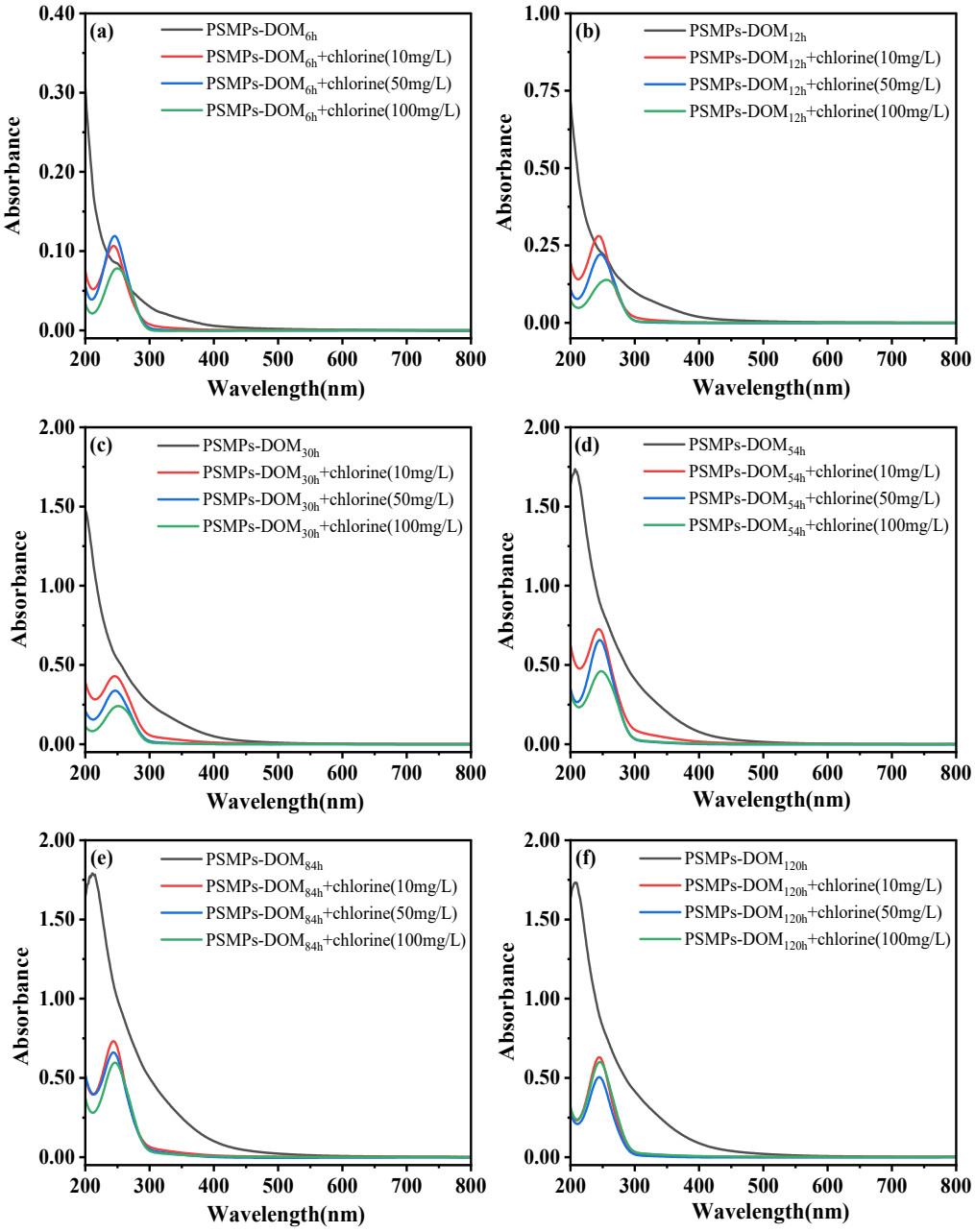

Fig. S7 UV-vis spectra of PSMPs-DOM before and after chlorination

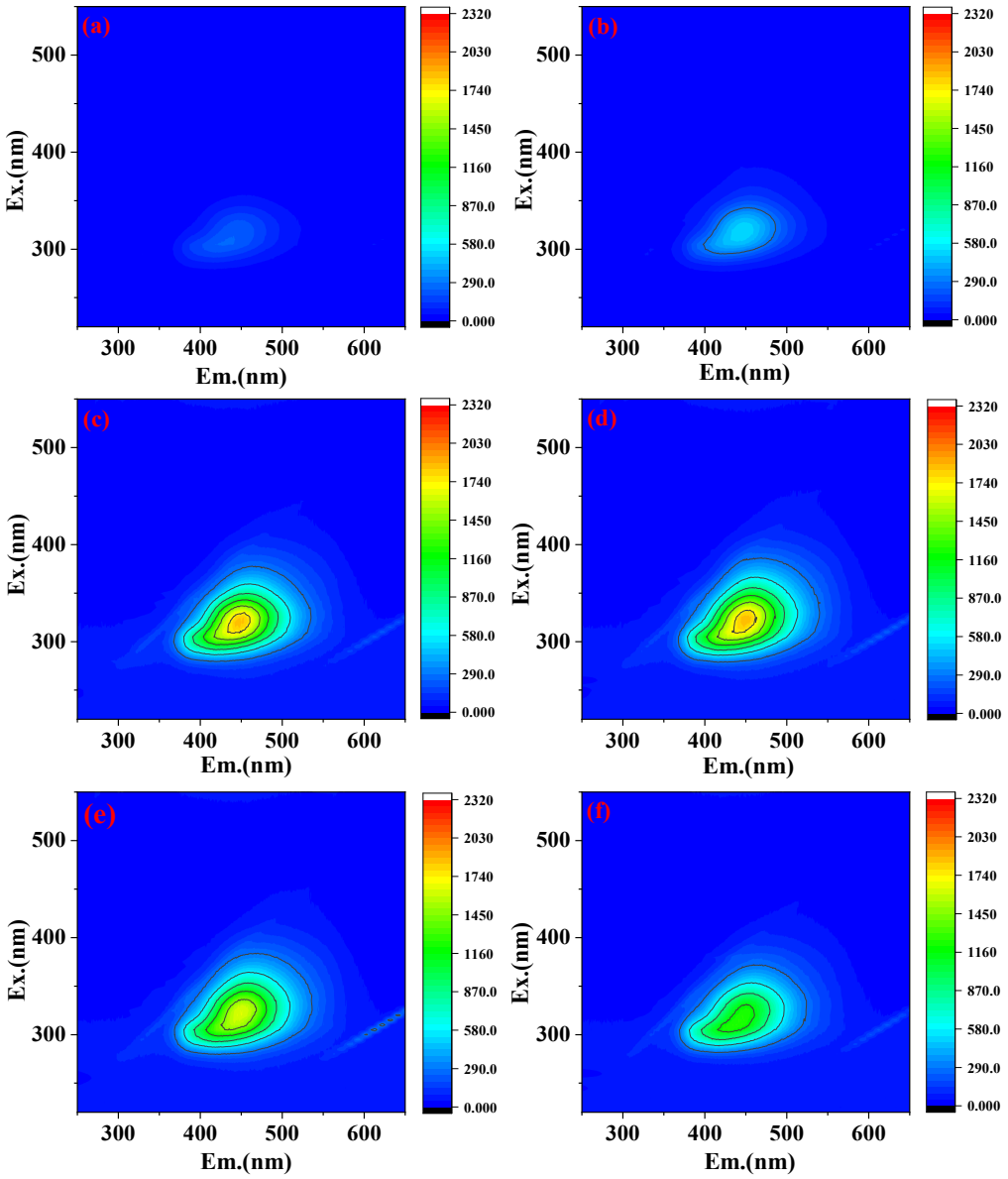

Fig. S8 EEM spectra of PSMPs-DOM$_x$ under 10 mg/L chlorination ((a)-(f), x = 6, 12, 30, 54, 84, 120 h)

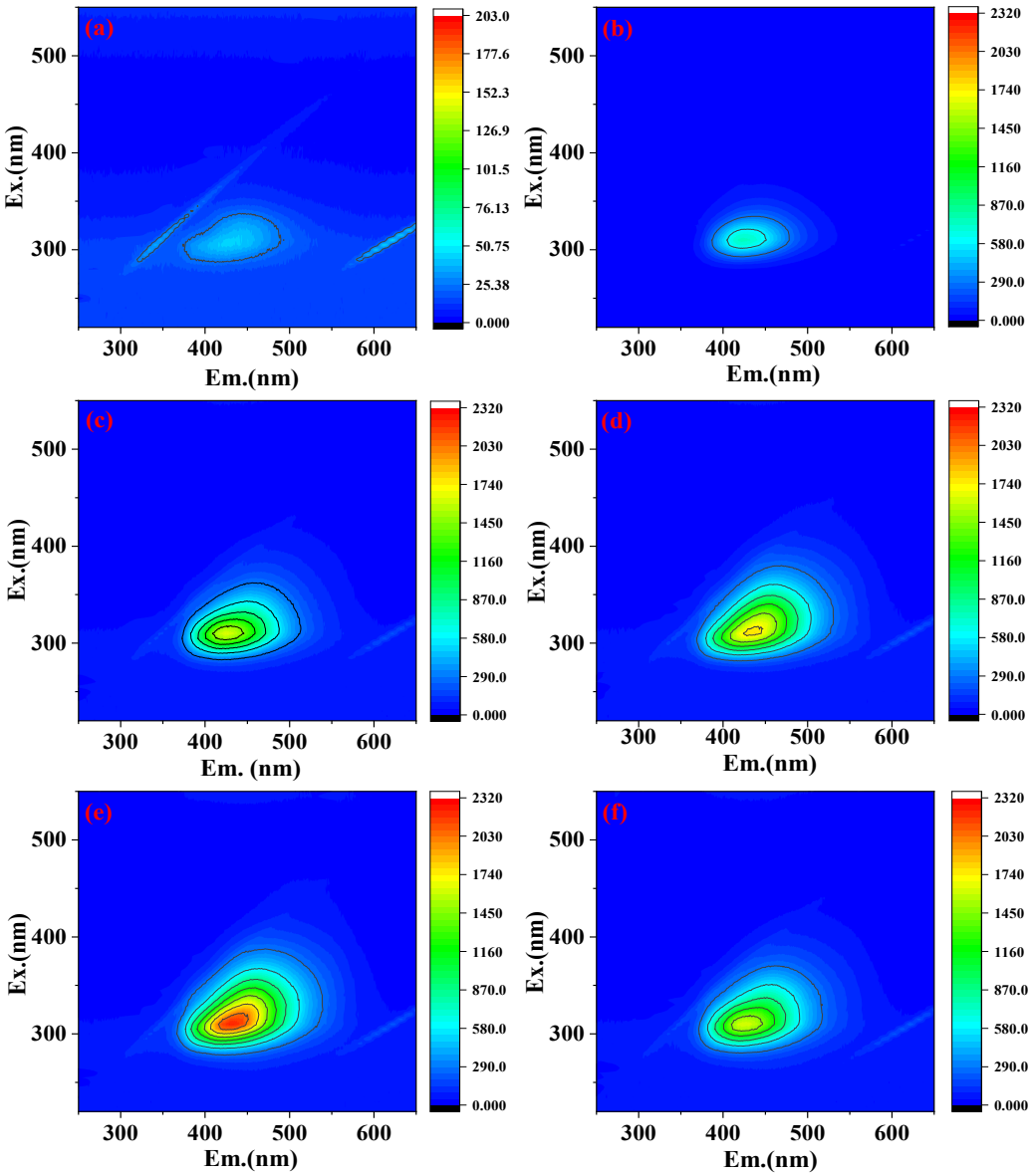

Fig. S9 EEM spectra of PSMPs-DOM$_x$ under 50 mg/L chlorination ((a)-(f), x = 6, 12, 30, 54, 84, 120 h)

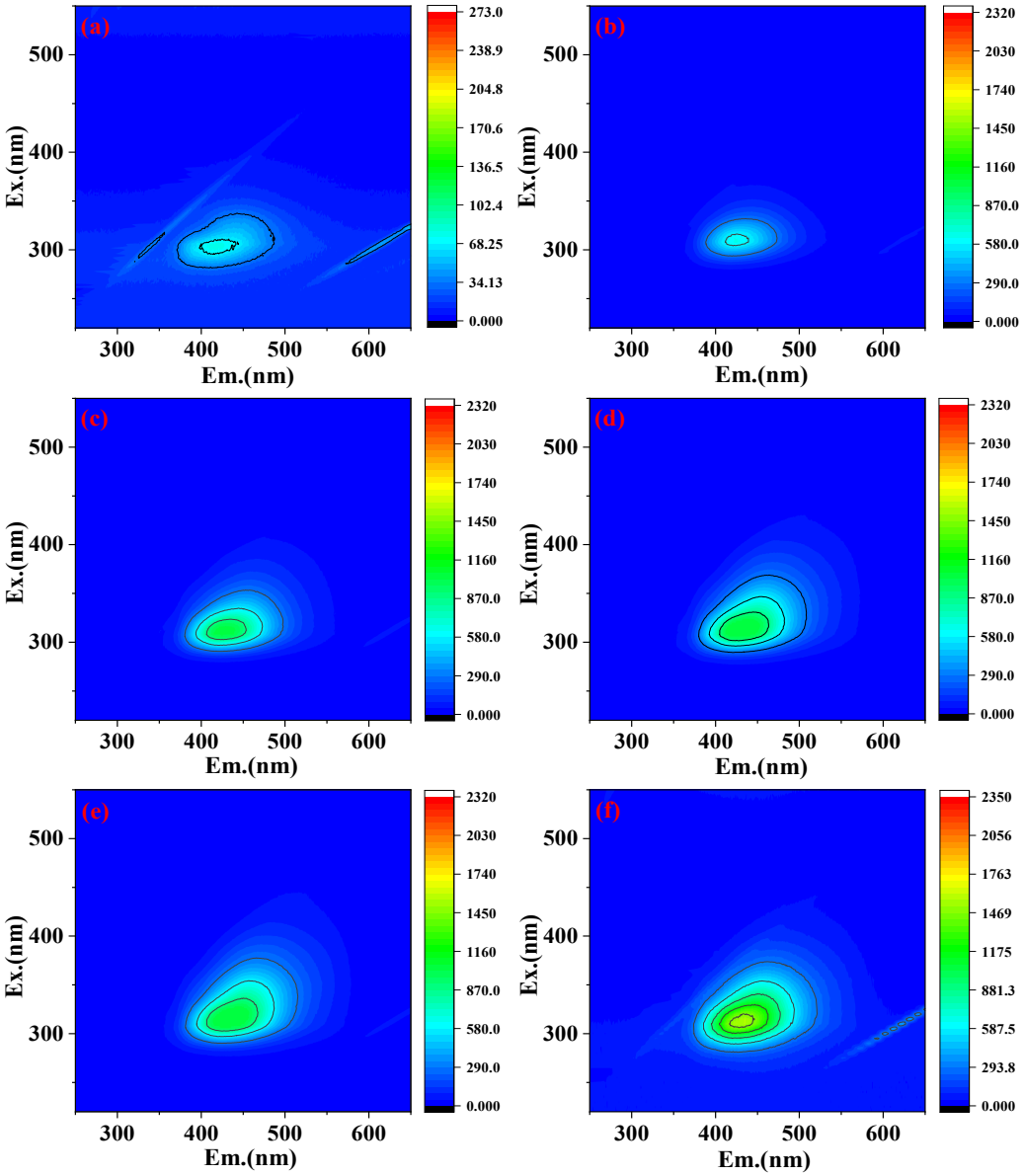

Fig. S10 EEM spectra of PSMPs-DOM$_x$ under 100 mg/L chlorination ((a)-(f), x = 6, 12, 30, 54, 84, 120 h)

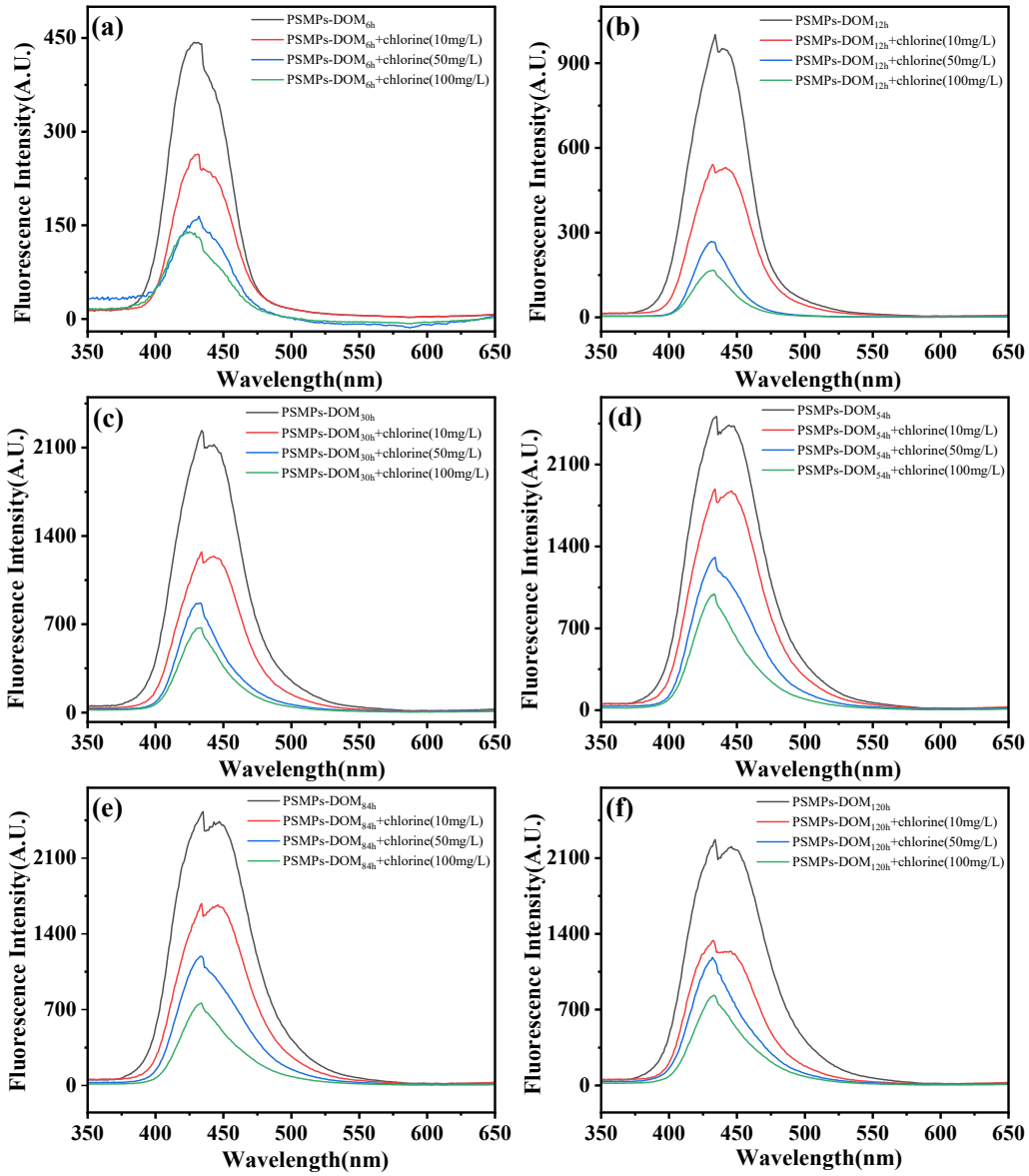

Fig. S11 Synchronous fluorescence spectra of PSMPs-DOM before and after chlorination

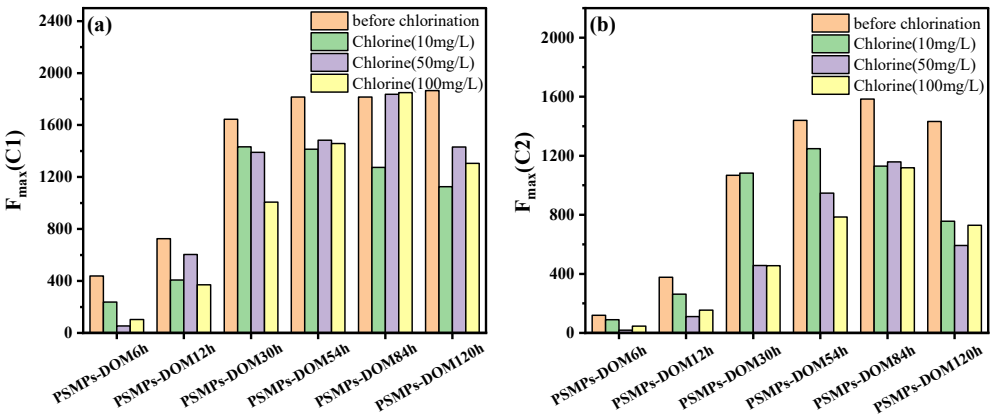

152

153 Fig. S12 F_{max}(C1) (a) and F_{max}(C2) (b) of PSMPs-DOM before and after chlorination

154

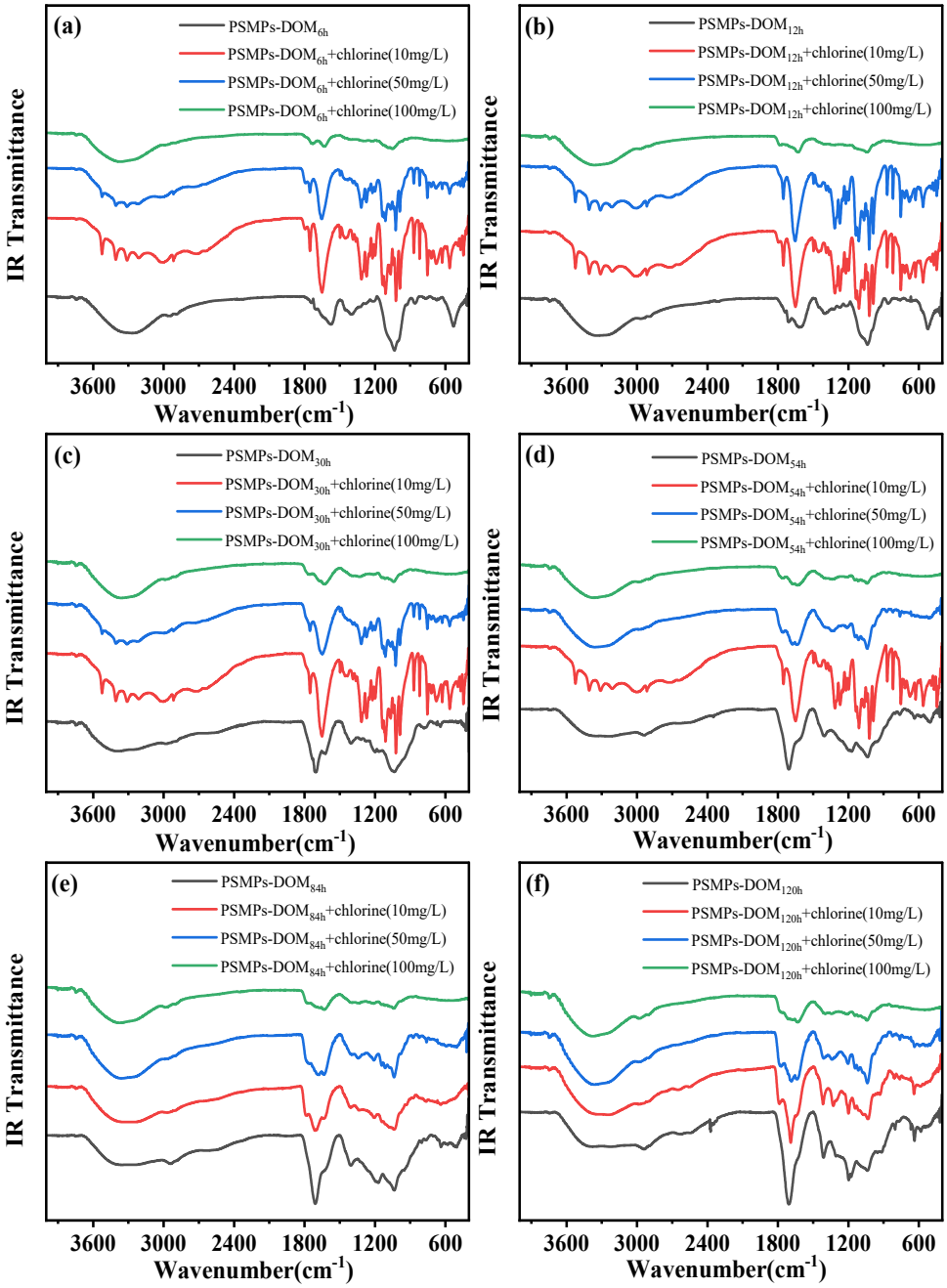

Fig. S13 FTIR spectra of PSMPs-DOM before and after chlorination

Table S1. Analytical methods of THMs by GC-ECD

GC/ECD	Agilent Technologies 7820A, USA
Column types	HP-5, 30 m × 0.32 mm × 0.25 μm
Split ratio	Splitless
Injection volume	1 μL
Injection Temperature	200°C
Oven temperature and ramp	The initial temperature of 30°C for 10.5 min, then an increase of 14°C/min to 72°C, which was held for 1 min, and finally an increase of 40°C to 200°C, which was held for 2 min.
Detector temperature	300°C
Carrier gas	N_2, constant flow at 3 mL/min

Table S2. The summary of Noda's rules for interpreting synchronous (Φ (ν1, ν2)) and asynchronous (ψ (ν1, ν2)) cross peaks in 2D-COS analysis (Noda et al., 2000).

sign at Φ (ν1, ν2)	sign at ψ (ν1, ν2)	interpretation
+		the intensity of ν1 and ν2 are changing in the same direction, i.e. increasing or decreasing together
-		the intensity of ν1 and ν2 are changing in the opposite direction
+	+	the change at ν1 is occurring predominantly before that at ν2
+	-	the change at ν1 is occurring predominantly after that at ν2
-	+	the change at ν1 is occurring predominantly after that at ν2
-	-	the change at ν1 is occurring predominantly before that at ν2

Table S3. Main absorption bands of PSMPs in the IR regions and their identifying assignment groups.

Wavenumber/ (cm^{-1})	Functional groups	References
3746	-OH	(Chen et al., 2020)
2973	-CH	(Zhang et al., 2020)
2902	$-CH_2$	(Zhang et al., 2020)
1730	C=O	(Wang et al., 2023)
1066	C-O	(Leng, 2018)

Table S4. DOC concentration of PSMPs-DOM under different UV irradiation time

Samples	UV irradiation time/ (h)	DOC/ (mg C/L)
PSMPs-DOM	6	8.71±0.17
	12	21.31±0.17
	30	68.33±0.21
	54	122.29±0.48
	84	184.62±0.05
	120	214.05±0.32

Table S5. UV parameters of PSMPs-DOM under different UV irradiation time

Samples	UV irradiation time/ (h)	α_{254}/ (m^{-1})	$S_{275-295}$/ (nm^{-1})
PSMPs-DOM	6	18.60±0.13	0.018±0.002
	12	49.43±0.18	0.016±0.005
	30	117.59±0.25	0.015±0.007
	54	184.12±0.10	0.015±0.004
	84	218.33±0.44	0.015±0.001
	120	179.84±0.19	0.014±0.002

Table S6. F_{max} value of PSMPs-DOM under different UV irradiation time

Samples	UV irradiation time/ (h)	F_{max}(C1)	F_{max}(C2)
PSMPs-DOM	6	438	119
	12	726	377
	30	1644	1068
	54	1815	1440
	84	1815	1585
	120	1866	1433

Table S7. $\Delta\alpha_{254}$ and $\Delta S_{275\text{-}295}$ of PSMPs-DOM after chlorination

Chlorine dosage/ (mg/L)	Samples	$\Delta\alpha_{254}$/ (m^{-1})	$\Delta S_{275\text{-}295}$/ ($nm^{-1}$)
10	$PSMPs\text{-}DOM_{6h}$	2.38±0.27	0.044±0.004
	$PSMPs\text{-}DOM_{12h}$	5.08±0.32	0.047±0.003
	$PSMPs\text{-}DOM_{30h}$	24.83±2.46	0.041±0.003
	$PSMPs\text{-}DOM_{54h}$	36.35±2.80	0.036±0.003
	$PSMPs\text{-}DOM_{84h}$	74.54±3.41	0.043±0.002
	$PSMPs\text{-}DOM_{120h}$	54.33±1.07	0.062±0.004
50	$PSMPs\text{-}DOM_{6h}$	5.86±0.26	0.071±0.004
	$PSMPs\text{-}DOM_{12h}$	1.81±0.33	0.074±0.006
	$PSMPs\text{-}DOM_{30h}$	44.96±0.30	0.061±0.005
	$PSMPs\text{-}DOM_{54h}$	47.21±0.83	0.064±0.003
	$PSMPs\text{-}DOM_{84h}$	86.03±0.91	0.050±0.002
	$PSMPs\text{-}DOM_{120h}$	78.71±1.05	0.069±0.002
100	$PSMPs\text{-}DOM_{6h}$	0.92±0.10	0.083±0.001
	$PSMPs\text{-}DOM_{12h}$	17.60±0.17	0.071±0.004
	$PSMPs\text{-}DOM_{30h}$	62.46±2.71	0.070±0.003
	$PSMPs\text{-}DOM_{54h}$	81.89±1.87	0.059±0.007
	$PSMPs\text{-}DOM_{84h}$	90.65±4.09	0.059±0.006
	$PSMPs\text{-}DOM_{120h}$	54.22±4.16	0.063±0.001

Table S8. Relative percentage of C1 and C2 in PSMPs-DOM before and after chlorination

Samples	Chlorine dosage/ (mg/L)	C1/ (%)	C2/ (%)
$PSMPs\text{-}DOM_{6h}$	0	78.61	21.39
	10	72.58	27.42
	50	73.83	26.17
	100	69.14	30.86
$PSMPs\text{-}DOM_{12h}$	0	65.80	34.20
	10	60.84	39.16
	50	84.51	15.49
	100	70.56	29.44
$PSMPs\text{-}DOM_{30h}$	0	60.62	39.38
	10	56.95	43.05
	50	75.27	24.73
	100	68.84	31.16
$PSMPs\text{-}DOM_{54h}$	0	55.76	44.24
	10	53.11	46.88
	50	61.02	38.98
	100	65.00	35.00
$PSMPs\text{-}DOM_{84h}$	0	53.39	46.61
	10	52.98	47.02
	50	61.33	38.67
	100	62.31	37.69
$PSMPs\text{-}DOM_{120h}$	0	56.57	43.43
	10	59.78	40.22
	50	70.74	29.26
	100	64.16	35.84

Table S9. Main absorption bands of PSMPs-DOM in the IR regions and their identifying assignment groups.

Samples	Wavenumber/ (cm^{-1})	Functional groups	References
$PSMPs\text{-}DOM_x$ (x=6,12,30,54h)	1654	Aromatic C=C/C=O	(Lee et al., 2021)
	1314	C-OH	(Leng, 2018)
	1270	C-O	(Zhang et al., 2022)
	1139	C-O-C	(Gu et al., 2024)
	1022	Aromatic C-H	(Lee et al., 2021)
$PSMPs\text{-}DOM_x$ (x=84,120h)	1721	O-C=O	(Liu et al., 2019)
	1139	C-O-C	(Gu et al., 2024)
	1022	Aromatic C-H	(Lee et al., 2021)

Table S10. 2D-FTIR-COS results of cross-peaks in synchronous and asynchronous maps

Group	Position/ (cm^{-1})	Sign						
PSMPs-DOM_{6h}		1754	1654	1300	1270	1111	1022	988
	1754	+	+(+)	+(+)	+(+)	+(+)	+(+)	+(+)
	1654		+	+(-)	+(+)	+(+)	+(+)	+(+)
	1300			+	+(+)	+(+)	+(+)	+(+)
	1270				+	+(+)	+(+)	+(+)
	1111					+	+(+)	+(+)
	1022						+	+(+)
	988							+
PSMPs-DOM_{12h}		1754	1654	1300	1270	1111	1022	988
	1754	+	+(-)	+(-)	+(-)	+(+)	+(+)	+(+)
	1654		+	+(-)	+(-)	+(+)	+(+)	+(+)
	1300			+	+(+)	+(+)	+(+)	+(+)
	1270				+	+(+)	+(+)	+(+)
	1111					+	+(+)	+(+)
	1022						+	+(-)
	988							+
PSMPs-DOM_{30h}		1754	1654	1300	1270	1111	1022	988
	1754	+	+(-)	+(-)	+(-)	+(-)	+(+)	+(+)
	1654		+	+(-)	+(+)	+(+)	+(+)	+(+)
	1300			+	+(+)	+(+)	+(+)	+(+)
	1270				+	+(-)	+(+)	+(+)
	1111					+	+(+)	+(+)
	1022						+	+(+)
	988							+
PSMPs-DOM_{54h}		1754	1654	1300	1270	1111	1022	988
	1754	+	+(+)	+(+)	+(+)	+(+)	+(+)	+(+)
	1654		+	+(+)	+(+)	+(+)	+(+)	+(+)
	1300			+	+(+)	+(-)	+(-)	+(+)
	1270				+	+(-)	+(-)	+(-)
	1111					+	+(+)	+(+)
	1022						+	+(+)
	988							+
PSMPs-DOM_{84h}		1709	1173	1032				
	1709	+	+(+)	+(-)				
	1173		+	+(-)				
	1032			+				
PSMPs-DOM_{120h}		1709	1173	1032				
	1709	+	+(+)	+(+)				
	1173		+	+(+)				
	1032			+				

Table S11. Formation potential of each THMs and total THMs in chlorinated PSMPs-DOM

Chlorine dosage/ (mg/L)	Samples	TCM/ (μg/mg C)	DCBM/ (μg/mg C)	DBCM/ (μg/mg C)	TBM/ (μg/mg C)	total THMs/ (μg/mg C)
10	PSMPs-DOM$_{6h}$	4.72±0.08	2.35±0.017	2.31±0.005	1.30±0.010	10.68±0.10
	PSMPs-DOM$_{12h}$	1.00±0.007	0.86±0.003	1.03±0.001	0.55±0.001	3.43±0.005
	PSMPs-DOM$_{30h}$	0.23±0.002	0.28±0.002	0.45±0.009	0.19±0.004	1.16±0.006
	PSMPs-DOM$_{54h}$	0.12±0.001	0.16±0.003	0.27±0.005	0.11±0.007	0.66±0.004
	PSMPs-DOM$_{84h}$	0.01±0.003	0.10±0.003	0.16±0.002	0.14±0.002	0.42±0.002
	PSMPs-DOM$_{120h}$	0.01±0.004	0.09±0.004	0.14±0.001	0.13±0.002	0.37±0.001
50	PSMPs-DOM$_{6h}$	15.99±0.01	2.10±0.003	1.55±0.003	0.94±0.003	20.58±0.02
	PSMPs-DOM$_{12h}$	7.95±0.08	0.98±0.007	0.95±0.001	0.60±0.007	10.48±0.09
	PSMPs-DOM$_{30h}$	0.93±0.02	0.39±0.001	0.43±0.001	0.28±0.002	2.02±0.02
	PSMPs-DOM$_{54h}$	0.28±0.004	0.17±0.002	0.27±0.004	0.13±0.008	0.85±0.01
	PSMPs-DOM$_{84h}$	0.17±0.005	0.13±0.001	0.20±0.002	0.13±0.005	0.63±0.006
	PSMPs-DOM$_{120h}$	0.12±0.003	0.12±0.001	0.15±0.003	0.14±0.007	0.53±0.008
100	PSMPs-DOM$_{6h}$	21.10±0.39	2.52±0.02	1.59±0.002	1.09±0.032	26.30±0.39
	PSMPs-DOM$_{12h}$	13.52±0.17	1.53±0.02	1.20±0.001	0.81±0.012	17.06±0.14
	PSMPs-DOM$_{30h}$	2.79±0.07	0.57±0.004	0.50±0.001	0.32±0.011	4.17±0.08
	PSMPs-DOM$_{54h}$	0.75±0.02	0.24±0.003	0.33±0.003	0.16±0.001	1.48±0.02
	PSMPs-DOM$_{84h}$	0.49±0.01	0.15±0.002	0.21±0.005	0.10±0.002	0.96±0.02
	PSMPs-DOM$_{120h}$	0.36±0.005	0.12±0.004	0.14±0.002	0.08±0.002	0.70±0.004

References:

Chen, W., Ding, S., Lin, Z., Peng, Y., Ni, J., 2020. Different effects of N2-flow and air-limited pyrolysis on bamboo-derived biochars' nitrogen and phosphorus release and sorption characteristics. Science of The Total Environment 711, 134828. https://doi.org/10.1016/j.scitotenv.2019.134828

Gu, X., Chen, B., Liu, H., Feng, Y., Wang, B., He, S., Feng, M., Pan, G., Han, S., 2024. Photochemical behavior of dissolved organic matter derived from Alternanthera philoxeroides hydrochar: Insights from molecular transformation and photochemically reactive intermediates. Journal of Hazardous Materials 461, 132591. https://doi.org/10.1016/j.jhazmat.2023.132591

Lee, Y.K., Hong, S., Hur, J., 2021. Copper-binding properties of microplastic-derived dissolved organic matter revealed by fluorescence spectroscopy and two-dimensional correlation spectroscopy. Water Research 190, 116775. https://doi.org/10.1016/j.watres.2020.116775

Leng, E., 2018. In situ structural changes of crystalline and amorphous cellulose during slow pyrolysis at low temperatures.

Liu, S., Feng, W., Song, F., Li, T., Guo, W., Wang, B., Wang, H., Wu, F., 2019. Photodegradation of algae and macrophyte-derived dissolved organic matter: A multi-method assessment of DOM transformation. Limnologica 77, 125683. https://doi.org/10.1016/j.limno.2019.125683

Noda, I., Dowrey, A.E., Marcott, C., Story, G.M., Ozaki, Y., n.d. Generalized Two-Dimensional Correlation Spectroscopy.

Wang, H., Zhu, J., He, Y., Wang, J., Zeng, N., Zhan, X., 2023. Photoaging process and mechanism of four commonly commercial microplastics. Journal of Hazardous Materials 451, 131151. https://doi.org/10.1016/j.jhazmat.2023.131151

Zhang, H., Chen, W., Li, Q., Zhang, X., Wang, C., Yang, L., Wei, R., Ni, J., 2020. Difference in characteristics and nutrient retention between biochars produced in nitrogen-flow and air-limitation atmospheres. J of Env Quality 49, 1396–1407. https://doi.org/10.1002/jeq2.20133

Zhang, H., Qian, W., Wu, L., Yu, S., Wei, R., Chen, W., Ni, J., 2022. Spectral characteristics of dissolved organic carbon (DOC) derived from biomass pyrolysis: Biochar-derived DOC versus smoke-derived DOC, and their differences from natural DOC. Chemosphere 302, 134869. https://doi.org/10.1016/j.chemosphere.2022.134869